Duan *et al. Chem. Biol. Technol. Agric.* (2024) 11:24
https://doi.org/10.1186/s40538-024-00548-2

Chemical and Biological Technologies in Agriculture

RESEARCH

Open Access

Transcriptome analysis reveals the potential mechanism of altering viability, yield, and isoquinoline alkaloids in *Coptis chinensis* through *Cunninghamia lanceolata* understory cultivation

Yuanyuan Duan[1,2,3†], Jingmao You[1,3†], Jintao Wang[1], Tao Tang[1,3], Xiaoliang Guo[1], Fanfan Wang[1,3], Xiaoyue Wang[1,2], Sen Mu[1], Qingfang Wang[1*], Xiaofeng Niu[4*] and Jie Guo[1,3*]

Abstract

The dried rhizomes of *Coptis chinensis* hold significance in Chinese medicine. Monocropping *C. chinensis* under the shade of a manmade scaffold, the primary planting mode, poses a threat to the ecological balance. In recent years, the practice of *C. chinensis–Cunninghamia lanceolata* understory cultivation has gained prevalence in southwest China. However, there is no evidence to suggest that understory cultivation enhances the viability, yield, or isoquinoline alkaloid content of *C. chinensis*. This study examined the physiological properties, yield indicators, and isoquinoline alkaloid content to investigate variations in *C. chinensis* in response to understory cultivation. Transcriptome analysis was conducted to elucidate potential mechanisms driving these alterations. The results indicate that understory cultivation significantly enhances the viability, yield, and levels of epiberberine, palmatine, and berberine in *C. chinensis* while reducing coptisine content. Transcriptomic analyses identified 2062 upregulated and 1853 downregulated genes in the understory cultivation system. Pathways such as "phenylpropanoid biosynthesis," "zeatin biosynthesis," "photosynthesis," "tyrosine metabolism," "isoquinoline alkaloid biosynthesis," and "starch and sucrose metabolism" exhibited significant enrichment of differentially expressed genes (DEGs). DEGs involved in these pathways were thoroughly analyzed. *INV*, *BGL-2*, *BGL-4*, *SPS-2*, *AMY-3*, *Psb B*, *Psb R*, *Psb S*, *Psa D*, *Psa E*, *Psa H*, *Psa O*, *Pet C*, *Pet H*, *deta*, and *b* exhibited significant positive correlations with plant fresh weight, aboveground fresh weight, and underground fresh weight. *6-OMT-2* and *COMT1-3* displayed significant positive correlations with coptisine content, but negative correlations with epiberberine, palmatine, and berberine content. *ZOG-1*, *ZOG-3*, *TAT*, *PPO*, *POD-13* and *UGT 73C5-1* showed noteworthy positive correlations with berberine content. Conversely, *MIFH*, *POD-4*, *POD-5*, and *POD-8* displayed significant positive correlations with epiberberine, palmatine, and berberine content. *POD-5*, and *POD-7* were significantly negatively correlated with coptisine content. Furthermore, gene expression levels determined by qRT–PCR aligned with the transcriptomic sequencing results, confirming the reliability of the transcriptomic

†Yuanyuan Duan and Jingmao You contributed equally to this work.

*Correspondence:
Qingfang Wang
qingfw0903@163.com
Xiaofeng Niu
niuxf@mail.xjtu.edu.cn
Jie Guo
gjms91@126.com
Full list of author information is available at the end of the article

findings. The results of this study contribute evidence elucidating potential mechanisms through which *C. chinensis* responds to understory cultivation.

Keywords *Coptis chinensis*, *Cunninghamia lanceolata*, Understory cultivation, Transcriptome, Yield, Isoquinoline alkaloids

Graphical Abstract

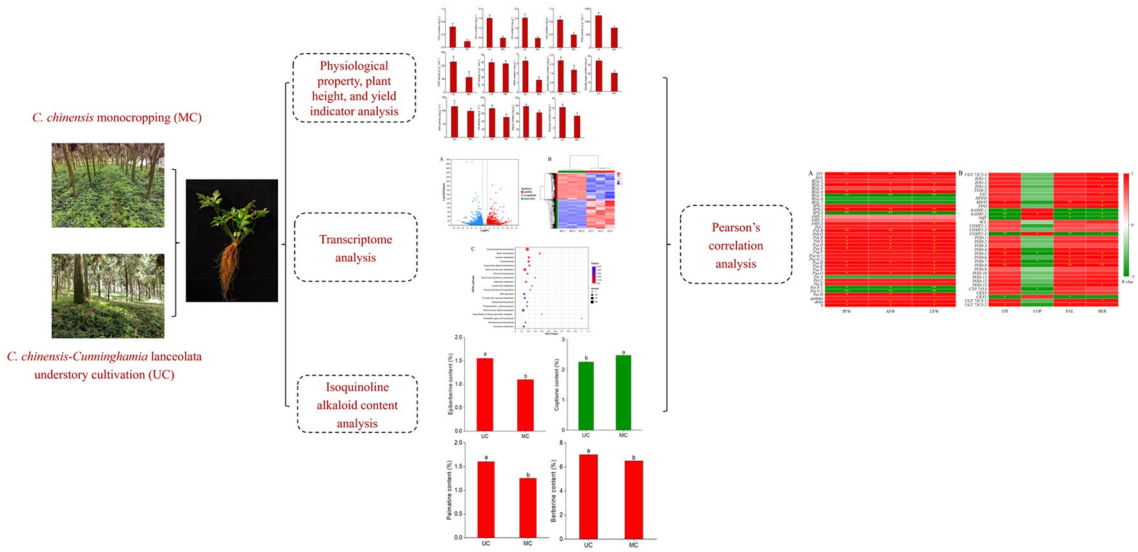

Introduction

Coptis chinensis Franch., a member of the Ranunculaceae family, stands as a pivotal medicinal plant [1]. The dried rhizomes of *C. chinensis*, known as "Weilian" in Chinese, found widespread use for purging fire, detoxication, and their antioxidant properties [2]. The primary active components of *C. chinensis* include isoquinoline alkaloids, such as epiberberine, palmatine, berberine, and coptisine [3]. With an annual output of 4000 tons, *C. chinensis* is extensively cultivated in southwest China [4], and its utilization has expanded into functional foods, beverages, and various products [5], leading to a significant rise in demand. However, the prevailing practice of monocropping *C. chinensis* under the shade of manmade scaffolds has been detrimental to the environment [6]. Continuous monocropping cultivation has resulted in a large-scale production reduction and diminished the quality of *C. chinensis* [4].

Understory cultivation emerges as a crucial agroforestry practice fostering increased biodiversity, the ecological balance, and enhanced crop quality [7, 8]. The complementarity in traits, timing, and spatial utilization between crops in the understory cultivation system plays a pivotal role in elevating crop quality [9, 10]. In the case of *C. chinensis*, the tall trees *Cunninghamia lanceolata* (Lamb.) Hooks, provide natural shade for *C. chinensis*, obviating the need for artificial scaffolds. Therefore, the *C. chinensis*–*C. lanceolata* understory cultivation (UC) pattern has been adopted in Lichuan, Hubei province. A prior study demonstrated that understory cultivation systems could enhance the yield and quality of *Fritillaria hupehensis* [11]. However, it remains uncertain whether this approach can similarly improve the yield of isoquinoline alkaloids, lacking the scientific evidence.

In recent years, integrative analyses combining physiological–chemical properties and transcriptomic sequencing have been employed to identify genes associated with yield and accumulation of secondary metabolite, predicting their functions [12]. Liu et al. analyzed the *C. chinensis* genome [13], and Chen et al. identified the genes linked to isoquinoline alkaloid biosynthesis [1]. However, the crucial genes governing the yield and isoquinoline alkaloid biosynthesis in response to understory cultivation remain poorly understood.

This study evaluated the physiological properties, yield indicators, and isoquinoline alkaloid content to discern

alterations in *C. chinensis* under understory cultivation with *C. lanceolata*. Subsequent transcriptomic sequencing reveled gene expression variations crucial for enhancing viability, yield, and isoquinoline alkaloid production. Pearson's correlation analysis identified candidate genes associated with the response to understory cultivation, predicting the relationships between gene expression and yield indicators/isoquinoline alkaloid content. These findings of novel insights into potential mechanisms that enhance the viability, yield, and isoquinoline alkaloid content of *C. chinensis* under understory cultivation systems.

Materials and methods

Plant materials and experimental design

The experiment took place in Jianzhuxi, Lichuan, Hubei Province, China (108° 33′ 21″ E, 30° 23′ 38′′ N, altitude 1530 m). Two cropping systems, *C. chinensis* monocropping (MC) and UC, were investigated. In the UC system, *C. chinensis* seedlings were planted within a 20-year-old *C. lanceolata* plantation with a plant row spacing of 2 × 3 m. In the MC system, *C. chinensis* seedlings were planted in the shade of a man-made scaffold using wooden stakes. *C. chinensis* seedlings, graded before testing, comprised 2-year-old healthy seedlings of similar sizes (± 20% errors). On May 18, 2021, *C. chinensis* seedlings were sown with a row spacing of 10 × 10 cm in both the MC and UC systems. The experiment, conducted in three replicates for MC and UC systems, had a plot size of 6.67 m^2 (1.50 × 4.45 m), and all plots were maintained following a conventional management model.

On February 13, 2022, young leaves were collected from three independent *C. chinensis* plants and combined as one biological duplicate for the UC and MC systems, respectively. Each system underwent three biological replicates. Leaves, frozen in liquid nitrogen and stored at − 80 °C, were used for RNA extraction. In addition, on June 13, 2022, 10 individual plants were randomly chosen from the UC and MC systems to measure plant height and fresh weight (yield indicators). Subsequently, fresh roots and plants were harvested. Fresh roots, washed and dried at 60 °C, were used to measure isoquinoline alkaloid contents, while fresh leaves utilized for measuring physiological properties.

Physiological property, plant height, and yield indicator measurements

Traditionally, *C. chinensis* rhizomes are harvested 5 years after planting for use in Chinese medicine [6]. This study selected plant fresh weight, aboveground fresh weight, and underground fresh weight as yield indicators. Plant height was measured using a 30 cm ruler, and plant, aboveground, and underground fresh weights were measured with an electronic (maximum range: 200 g). Values were averaged across 10 plants. Chlorophyll a (Chl a), chlorophyll b (Chl b), Chl a + Chl b (Chl), carotenoid (Car), peroxidase (POD), superoxide dismutase (SOD), catalase (CAT), malondialdehyde (MDA), soluble protein, and soluble sugar content were measured following the procedures outlined by Li et al. [13]. Starch and sucrose content, sucrose phosphate synthase (SPS), and sucrose synthase (SS, synthetic direction) activities were evaluated as described by Shi et al. [14].

Isoquinoline alkaloid content measurements

The isoquinoline alkaloids, including epiberberine, palmatine, and berberine, were prepared following previously established procedures [2]. The isoquinoline alkaloid contents were determined using a high-performance liquid chromatography (HPLC) system (Agilent 1260, Agilent Technologies, Germany) equipped with an Agilent C-18 chromatographic column (5 μm, 4.6 × 250 mm). The mobile phase and HPLC conditions were set according to the protocol outlined by Liu et al. [2].

Transcriptome analysis

Transcriptomic sequencing was performed by Shanghai Majorbio Bio-Pharm Biotechnology Co. Ltd. (Shanghai, China). Total RNA was extracted from *C. chinensis* leaves following the instructions for TRIzol® Reagent (Invitrogen, USA). RNA purification and concentration detection were performed as previously described [11]. The construction of cDNA libraries utilized high-quality RNA, adhering to the manufacturer's instructions on an Illumina® Stranded mRNA Prep (Illumina, San Diego, CA, USA). Sequencing was performed using the Illumina NovaSeq 6000 platform (Illumina, San Diego, CA, USA). HISAT2 software was employed to align the clean reads with the reference *C. chinensis* genome [15], and aligned reads were assembled using StringTie software [16].

Differential expression analysis was conducted using DESeq2 [17], with gene expression levels calculated as fragments per kilobase million. Genes meeting the criteria $|\log_2(\text{fold change})| \geq 1$ and false discovery rate ≤ 0.05 were considered significantly differentially expressed genes (DEGs). The Kyoto Encyclopedia of Genes and Genomes (KEGG) enrichment analysis was performed using KOBAS software [18]. Transcription factor gene families (TFs) were evaluated using the PlantTFDB Database website (http://planttfdb.cbi.pku.edu.cn/).

All raw sequencing data were submitted to the Genome Sequence Archive database (https://ngdc.cncb.

ac.cn/gsub/) under the BioProject accession number CRA012562.

Quantitative reverse transcription–polymerase chain reaction analysis

Eight genes involved in isoquinoline alkaloid biosynthesis and the starch and sucrose metabolism pathways were randomly selected for real-time quantitative reverse transcription–polymerase chain reaction (qRT–PCR). The internal reference gene used was *18S rRNA* [19]. Primers were designed at https://bioinfo.ut.ee/primer3-0.4.0/, and the sequences are listed in Additional file 2: Table S1. qRT–PCR was performed as described in a previous study [19]. The $2^{-\triangle\triangle CT}$ method was used to calculate the relative expression levels with three biological and three technical replicates analyzed.

Statistical analyses

Statistical analyses were conducted using SPSS software version 19.0. Significant differences were assessed using a one-way analysis of variance and Duncan's multiple range test ($p < 0.05$). Column graphs and Pearson's correlation heat maps of gene expression levels, physiological properties, plant height, yield indicators, and isoquinoline alkaloid content were plotted using Origin Pro 2021 software. The TBTools software (version 1.068) was employed to illustrate the DEG heatmaps.

Results

Physiological properties, plant height, and yield indicators of *C. chinensis* in response to understory cultivation

In this study, we measured physiological properties and yield indicators to explore how *C. chinensis* responds to understory cultivation (Figs. 1, 2, Table 1). The UC group exhibited significantly higher Chl, Chl a, Chl b, and Car contents compared to the MC group ($p < 0.05$). In addition, POD, SOD, and SS enzyme activities, soluble protein and sugar content, starch and sucrose content, and MDA content exhibited significant increases in the UC group. Specifically, POD activity, SOD activity, SS activity, MDA content, and soluble sugar content rose by 62.08%, 102.68%, 43.86%, 154.86%, and 66.82% in UC, respectively, compared to MC. In addition, plant height, plant fresh weight, aboveground fresh weight, and underground fresh weight in the UC treatment saw significant increases of 101.29%, 44.68%, 40.26%, and 52.55%, respectively. These results indicate that understory cultivation increases the viability and yield of *C. chinensis*.

Fig. 1 Phenotypic changes of *C. chinensis* in MC and UC systems

Transcriptome sequencing, functional annotation, and differentially expressed gene analysis in *C. chinensis*

Illumina sequencing was employed to assess gene expression levels in the UC and MC leaf samples. An overview of the sequencing data is presented in Additional file 2: Table S2. The UC and MC samples yielded a total of 43,287,359 and 43,533,923 clean reads, with 86.58% and 86.94% uniquely mapped to the *C. chinensis* genomes, respectively. Moreover, the Q30 average values for the UC and MC samples were 94.56% and 94.65%, respectively, indicating satisfactory quality of transcriptome sequencing.

Functional annotations based on the GO databases were utilized to obtain comprehensive information on the assembled unigenes (Additional file 1: Fig. S1). A total of 3915 DEGs were classified into "biological process," "cellular component," and "molecular function." In the biological process category, DEGs (1856) were predominantly enriched in the "catalytic activity" GO term. For the cellular component category, the majority of unigenes (1438) were annotated in the "cell part" GO term. In the molecular function category, the "cellular process" (1206) and "metabolic process" (1123) were the most common.

Compared to MC, 2062 upregulated and 1853 downregulated genes were identified in UC (Fig. 3A). In addition, all DEGs were clustered into two groups that exhibited opposite expression patterns in the UC and MC systems (Fig. 3B). The KEGG enrichment analysis showed significant enrichment of genes in pathways such as "Phenylpropanoid biosynthesis (map00940)," "Zeatin biosynthesis (map00908)," "Tyrosine metabolism (map00350)," "Photosynthesis (map00195)," "Isoquinoline alkaloid biosynthesis (map00950)," and "Starch and sucrose metabolism (map00500)" pathways ($p$adjust < 0.05). This suggests their essential role in *C. chinensis* growth in response to understory cultivation systems (Fig. 3C). In addition, 375 differentially expressed TFs were identified in the transcriptome of *C. chinensis* and classified into 30 families. The top 10 TF families were

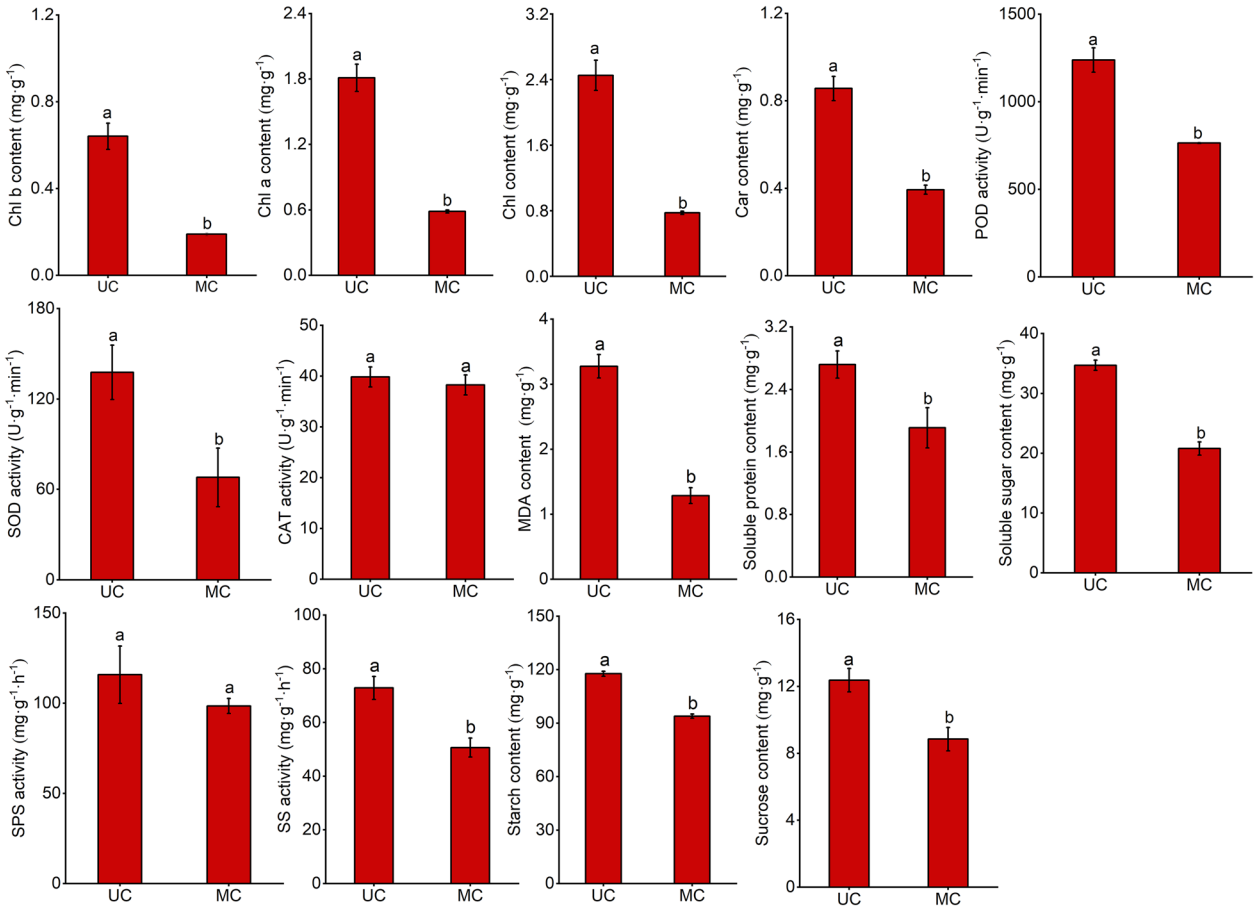

Fig. 2 Physiological properties of *C. chinensis* in UC and MC systems. All the data in the figure are presented as the mean ± standard error of the mean (SEM). Different letters in each system represent significant differences at $p < 0.05$. *Chl a* chlorophyll a, *Chl b* chlorophyll b, *Chl* chlorophyll a + chlorophyll b, *Car* carotenoid

Table 1 Plant height and yield indicators of *C. chinensis* in UC and MC systems

System	Plant height (cm)	Plant fresh weight (g)	Aboveground fresh weight (g)	Underground fresh weight (g)
UC	24.96 ± 0.38a	102.55 ± 1.76a	63.65 ± 1.31a	38.90 ± 0.51a
MC	12.40 ± 0.29b	70.88 ± 1.47b	45.38 ± 1.01b	25.50 ± 0.53b

The values in the table are expressed as mean ± SEM. Different letters within each system represent indicate differences at $p < 0.05$

ERF/DREB (17.5%), WRKY (11.0%), HD-ZIP (7.9%), MYB (7.9%), MIKC (7.6%), C4-GATA-related (4.5%), GARP_G2-like (4.5%), SBP (3.9%), DOF (3.6%), and AP2 (3.1%) (Additional file 1: Fig. S2).

Differentially expressed genes in the phenylpropanoid biosynthesis

In this study, 17 DEGs were identified in the phenylpropanoid biosynthesis pathway (map00940) (Fig. 4, Additional file 2: Table S3). In comparison with MC, one, two, and thirteen genes encoding 4-coumarate-CoA ligase (4CL), caffeic acid 3-*O*-methyltransferase (COMT1), and POD, respectively, were significantly upregulated in UC, consistent with the change in POD activity.

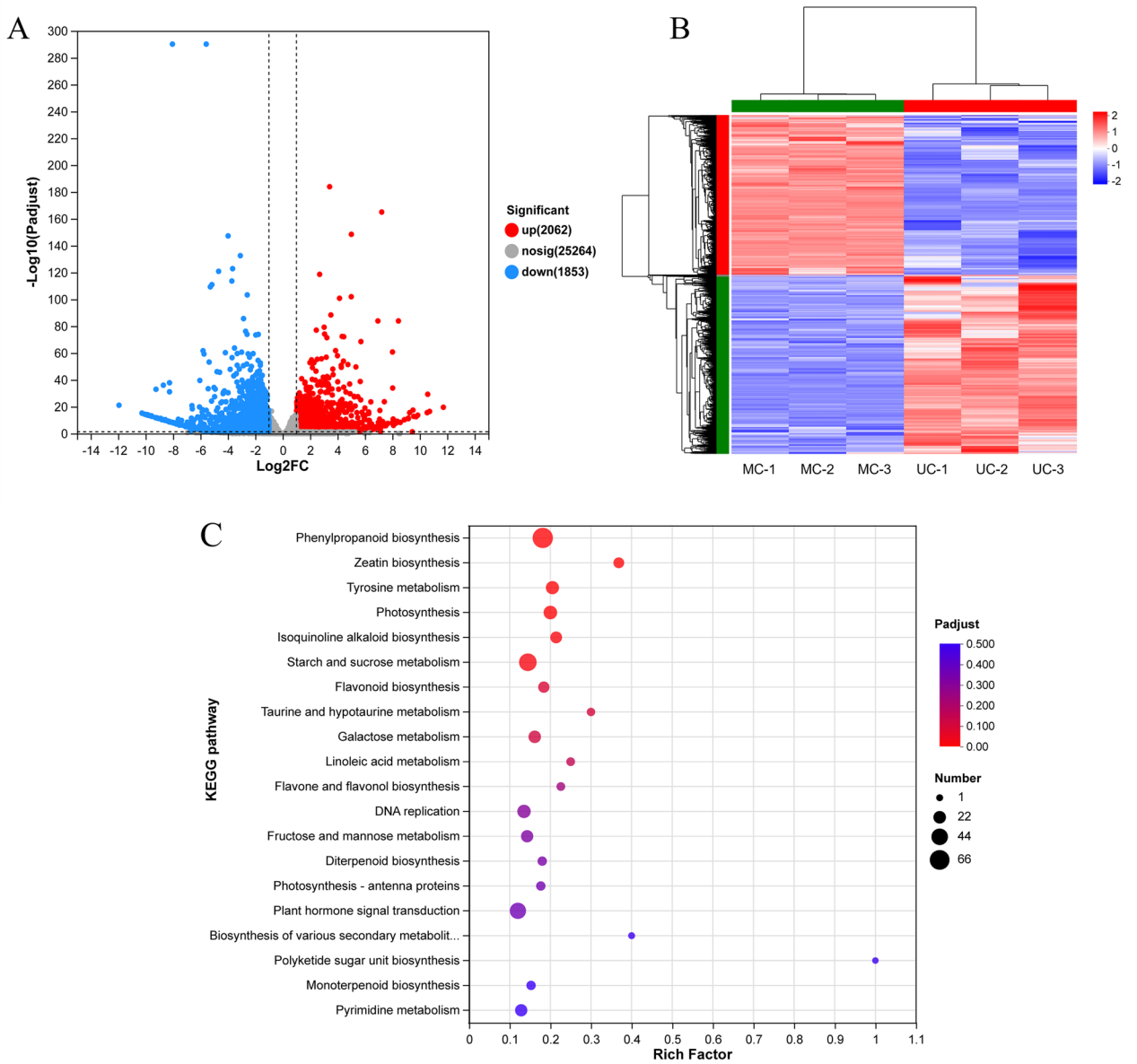

Fig. 3 Analysis of DEGs in "UC_vs_MC". **A** Volcano diagram of DEGs. **B** Hierarchical clustering diagram of DEGs. **C** KEGG enrichment analysis of DEGs

Differentially expressed genes in the zeatin biosynthesis

Nine DEGs involved in the zeatin biosynthesis pathway (map00908) were identified in "UC_vs_MC" (Fig. 5, Additional file 2: Table S4). Among these DEGs, one, one, three, and three genes encoding cytokinin hydroxylase (CYP 735A), cytokinin dehydrogenase 5 (CKX5), zeatin *O*-glucosyltransferase (ZOG), and UDP-glycosyltransferase 73C5 (UGT 73C5), respectively, were significantly upregulated in UC.

Differentially expressed genes in photosynthesis

After understory cultivation, a total of 22 DEGs related to the photosynthetic pathway (map00195) were identified (Fig. 6, Additional file 2: Table S5). Compared with MC, 20 of those genes encoding photosystem II CP47 reaction center protein (Psb B), oxygen-evolving enhancer protein 1 (Psb O), photosystem II 10 kDa polypeptide (Psb R), and photosystem II 22 kDa protein (Psb S) in the photosystem II reaction center, photosystem I reaction center subunit proteins (Psa D, Psa E, Psa F, Psa G, Psa H, Psa K, Psa N, and Psa O), cytochrome b6-f complex iron–sulfur subunit (Pet C), plastocyanin A (Pet E), and ferredoxin-3

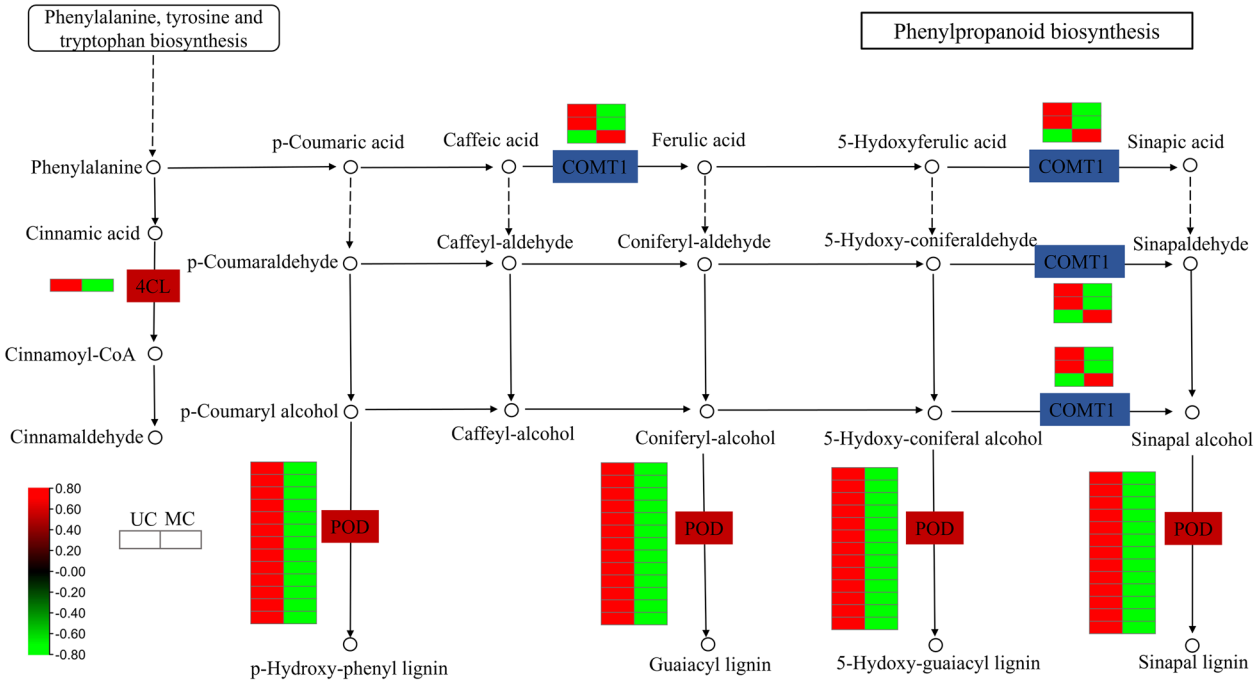

Fig. 4 DEGs in the phenylpropanoid biosynthesis pathway. Red frames indicate upregulated genes, green frames denote downregulated genes, and blue frames indicate up- and down-regulated genes in "UC_vs_MC". The relative expression levels of DEGs were calculated using the $\log_2$ ratio

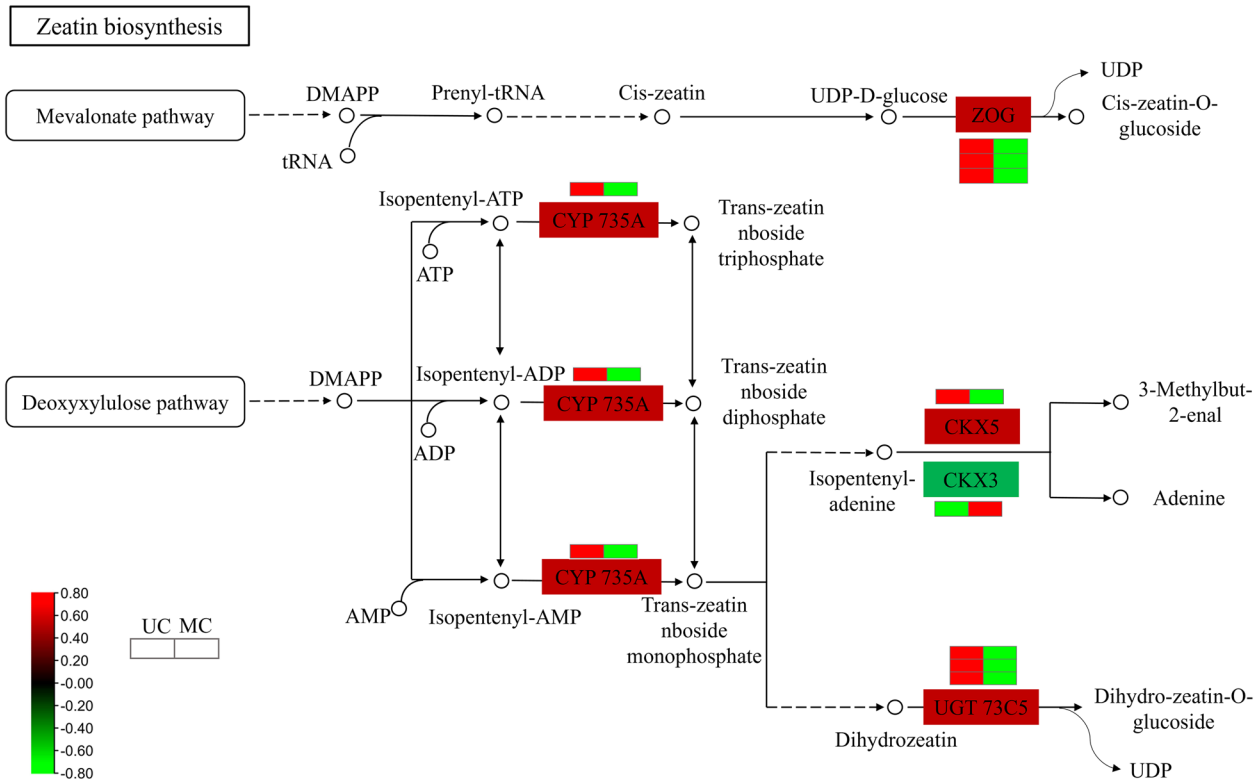

Fig. 5 DEGs in the zeatin biosynthesis pathway. Red frames denote upregulated genes and green frames denote downregulated genes in "UC_vs_MC". The relative expression levels of DEGs were calculated by the $\log_2$ ratio

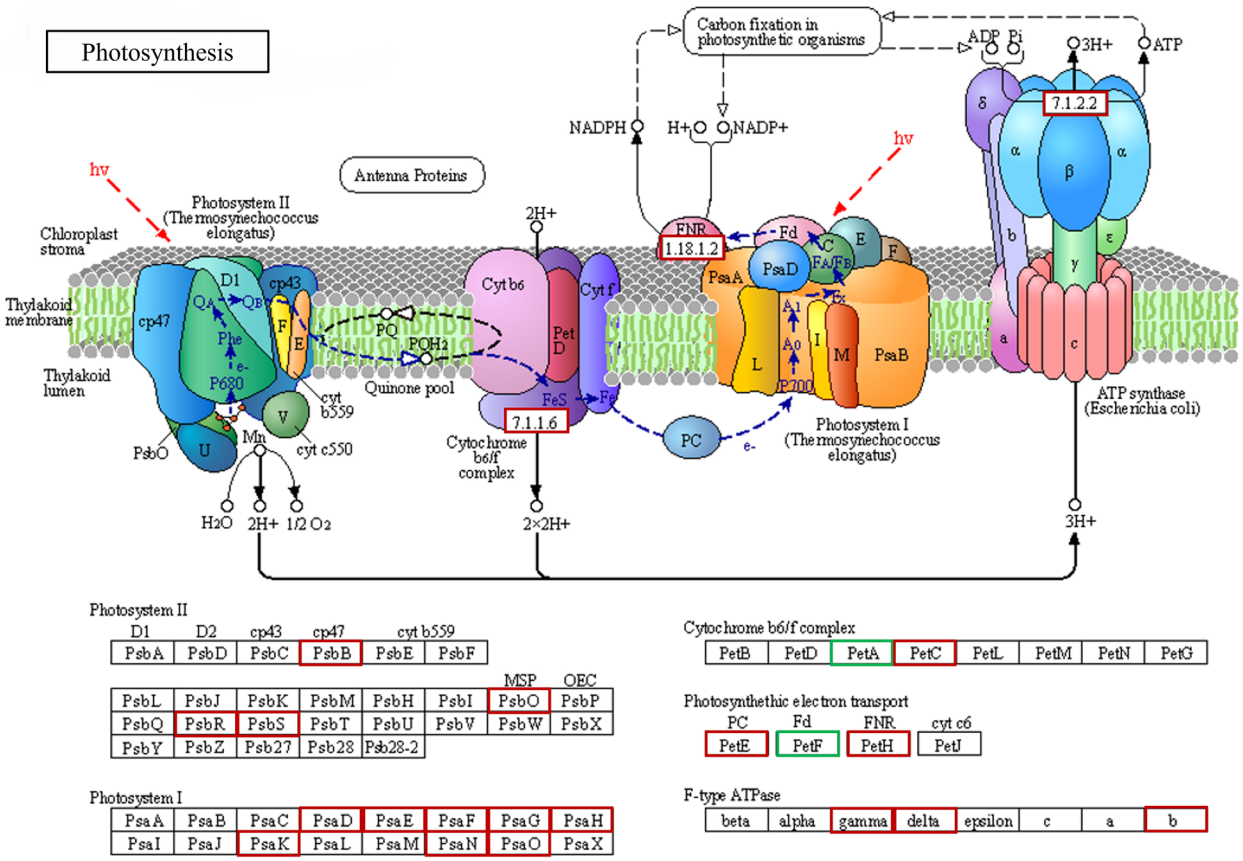

Fig. 6 DEGs in the photosynthesis pathway. Red frames denote upregulated genes and green frames denote downregulated genes in "UC_vs_MC". The relative expression levels of DEGs were calculated by $\log_2$ ratio

(Pet F) involved in photosynthetic electron transport, ATP synthase gamma chain (gamma), ATP synthase subunit delta (delta), and ATP synthase subunit *b*′ (*b*), were significantly upregulated in UC. These alternately expressed genes may play essential roles in *C. chinensis* photosynthesis in response to understory cultivation.

Differentially expressed genes in the tyrosine metabolism and isoquinoline alkaloid biosynthesis

Genes involved in tyrosine metabolism and isoquinoline alkaloid biosynthesis were found to be altered by understory cultivation. Eight DEGs were identified in tyrosine metabolism and isoquinoline alkaloid biosynthesis pathways (Fig. 7A, Additional file 2: Table S6). Compared with MC, one gene each encoding tyrosine aminotransferase (TAT), tyrosine/dopa decarboxylase 2 (TYDC2), and polyphenol oxidase (PPO) was significantly upregulated in UC in both the tyrosine metabolism and isoquinoline alkaloid biosynthesis pathways. In the tyrosine metabolism pathway, one gene encoding 4-hydroxyphenylpyruvate dioxygenase (HPPD) and one gene encoding the macrophage migration inhibitory factor homolog (MIFH) were significantly upregulated in UC. Two genes encoding (*S*)-norcoclaurine 6-*O*-methyltransferase (6-OMT) and one gene encoding (*S*)-scoulerine 9-*O*-methyltransferase (SMT) were significantly downregulated in UC.

In addition, the content of the four isoquinoline alkaloids was measured using HPLC (Fig. 7B–D). The epiberberine, palmatine, and berberine contents significantly increased by 41.27%, 27.80%, and 7.99%, respectively, in UC, whereas the coptisine level significantly decreased by 8.86% compared to MC.

Differentially expressed genes in the starch and sucrose metabolism

In the "UC_vs_MC" comparison, 16 DEGs were identified in the starch and sucrose metabolism pathways (Fig. 8, Additional file 2: Table S7). The results showed that one, one, four, two, three, and one genes encoding beta-fructofuranosidase (INV), alpha-glucosidase (AGL), beta-glucosidase (BGL), SPS, alpha-amylase (AMY), and

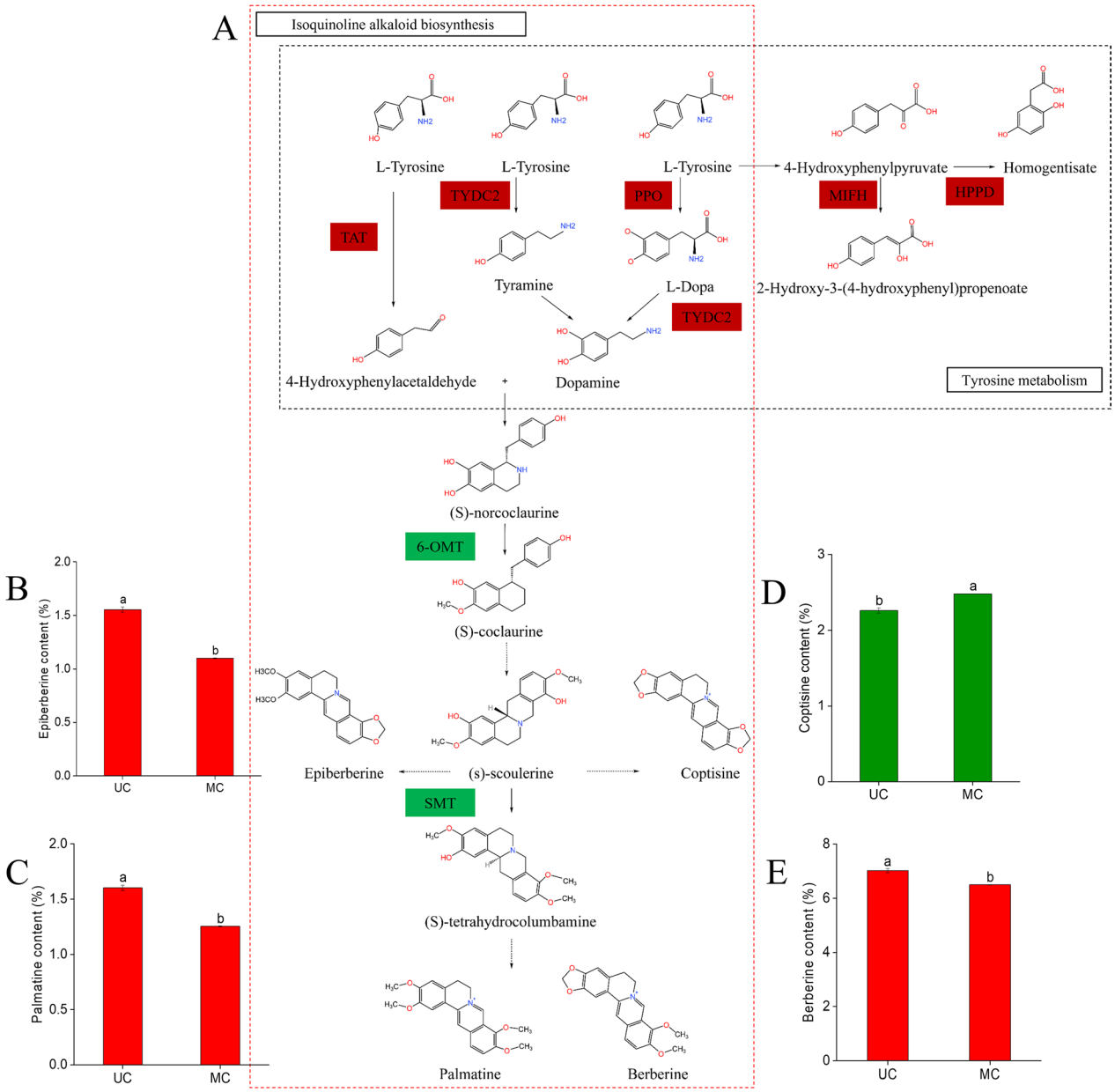

Fig. 7 Isoquinoline alkaloid contents and DEGs in tyrosine metabolism and the isoquinoline alkaloid biosynthesis pathway. **A** DEGs in tyrosine metabolism and the isoquinoline alkaloid biosynthesis pathway. Red frames indicate upregulated genes and green frames indicate downregulated genes in "UC_vs_MC". The relative expression levels of DEGs were calculated using the $\log_2$ ratio. **B**–**E** Isoquinoline alkaloid contents in the UC and MC systems

isoamylase (ISA) were significantly upregulated in UC compared to MC.

Integrated analyses of the physiological properties, yield indicators, isoquinoline alkaloid contents and transcriptome profile

In this study, Pearson's *r* values between DEGs and yield indicators/isoquinoline alkaloid contents were calculated (Fig. 9, Additional file 2: Tables S8, S9). *INV*, *BGL-2*, *BGL-4*, *SPS-2*, *AMY-3*, *Psb B*, *Psb R*, *Psb S*, *Psa D*, *Psa E*, *Psa H*, *Psa O*, *Pet C*, *Pet H*, *deta*, and *b* showed significant positive correlations with plant fresh weight, aboveground fresh weight, and underground fresh weight ($R > 0.85$, $p < 0.01$) (Fig. 9A). *6-OMT-2* ($R = 0.97$, $p < 0.01$) and *COMT1-3* ($R = 0.93$, $p < 0.01$) were significantly positively correlated with coptisine content, but negatively

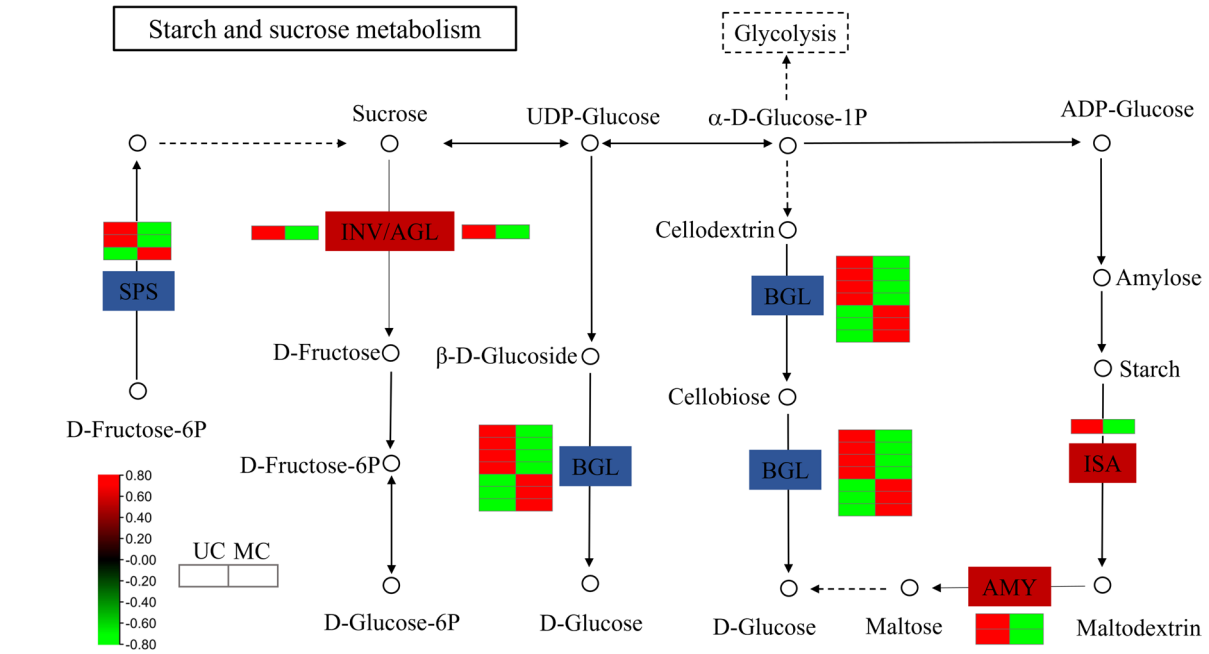

Fig. 8 DEGs in the starch and sucrose metabolism pathways. Red frames indicate upregulated genes and blue frames indicate up- and down-regulated genes in "UC_vs_MC". The relative expression levels of DEGs were calculated using the $\log_2$ ratio

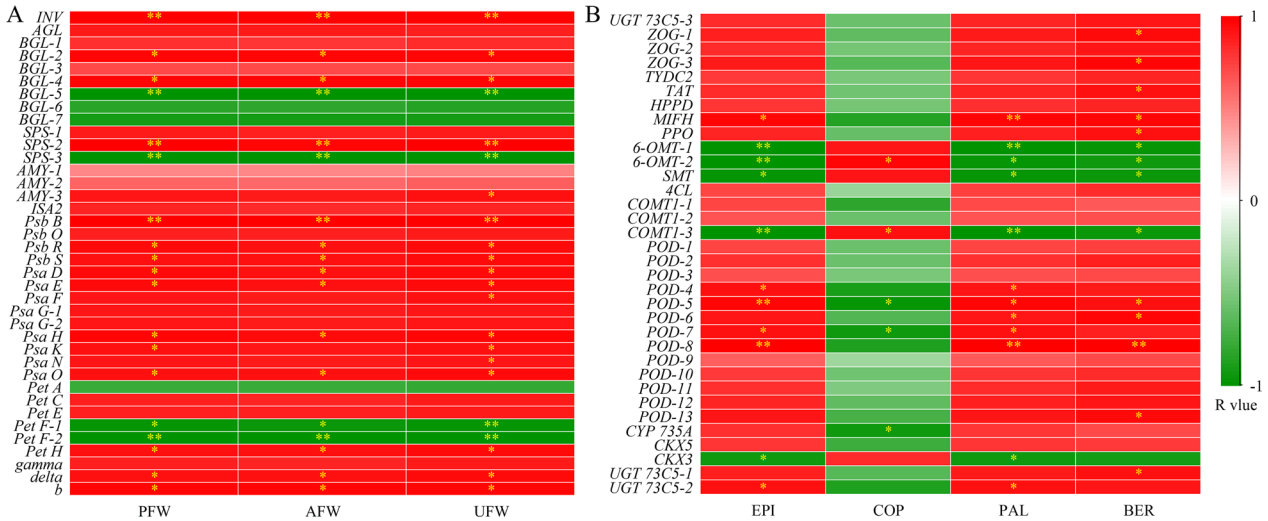

Fig. 9 Heatmaps of Pearson's correlations between DEGs and yield indicators (isoquinoline alkaloid contents). **A** Pearson's correlations between DEGs and yield indicators. **B** Pearson's correlations between DEGs and isoquinoline alkaloid contents. Pearson's *r* value was calculated (**$p < 0.01$; ***$p < 0.001$). *EPI* epiberberine content, *COP* coptisine content, *PAL* palmatine content, *BER* berberine content, *PFW* plant fresh weight, *AFW* aboveground fresh weight, *UFW* underground fresh weight

correlated with epiberberine, palmatine, and berberine content ($|R| > 0.93$, $p < 0.01$). *ZOG-1*, *ZOG-3*, *TAT*, *PPO*, *POD-13*, and *UGT 73C5-1* exhibited significant positively correlated with berberine content ($R > 0.83$, $p < 0.01$), and *MIFH*, *POD-4*, *POD-5*, and *POD-8* showed significant positively correlations with epiberberine, palmatine, and berberine content ($R > 0.92$, $p < 0.01$) (Fig.9B). In addition, *POD-5* and *POD-7* displaced significant negative correlations with coptisine content ($|R| > 0.81$, $p < 0.05$). The results showed that DEG expression levels may play essential roles in the accumulation of yield and isoquinoline alkaloids. In addition, SOD activity, POD activity,

MDA content, starch content, sucrose content, and SS activity were significantly positively correlated with epiberberine, palmatine, berberine ($R > 0.88$, $p < 0.05$) and negatively correlated with coptisine content ($|R| > 0.82$, $p < 0.05$) (Additional file 1: Fig. S3A). Moreover, Chl a, Chl b, Chl, Cars, soluble protein, soluble sugar content, starch content, sucrose content, and SS activity showed significant positive correlations with individual plant, aboveground, and underground fresh weights ($R > 0.87$, $p < 0.05$) (Additional file 1: Fig. S3B). The results showed that gene expression levels and alterations in physiological properties might play essential roles in isoquinoline alkaloid accumulation.

Validation of transcriptomic data using qRT–PCR

To validate the transcriptome results, eight genes were randomly selected for qRT–PCR analysis (Additional file 2: Table S10). As expected, the gene expression levels calculated using the $2^{-\triangle\triangle CT}$ were consistent with the RNA sequencing (RNA-seq) results (Fig. 10). In addition, linear regression analysis validated the reliability and accuracy of the RNA-seq results (Additional file 1: Fig. S4 and Additional file 2: Table S11).

Discussion

In the present study, chlorophyll and carotenoid content, plant height, and fresh weight were significantly higher in UC than in MC. Plant height and fresh weight are important growth and yield parameters [20], and chlorophyll and carotenoids play essential roles in light energy absorption and photosynthesis [21]. The substantial increase in these indicators under UC indicates a significant enhancement in the photosynthetic efficiency and overall yield of *C. chinensis*. Understory cultivation with *C. lanceolata* improves *C. chinensis* viability. In general, MDA is used to measure membrane peroxidation damage, and its value increases when crops are under stress [22]. Higher MDA levels in the MC indicated that *C. chinensis* in the understory cultivation system may have been subjected to stress. These stressors may cause cells in *C. chinensis* to produce superoxide-free radicals and induce antioxidant enzymes to reduce oxidative damage by preventing

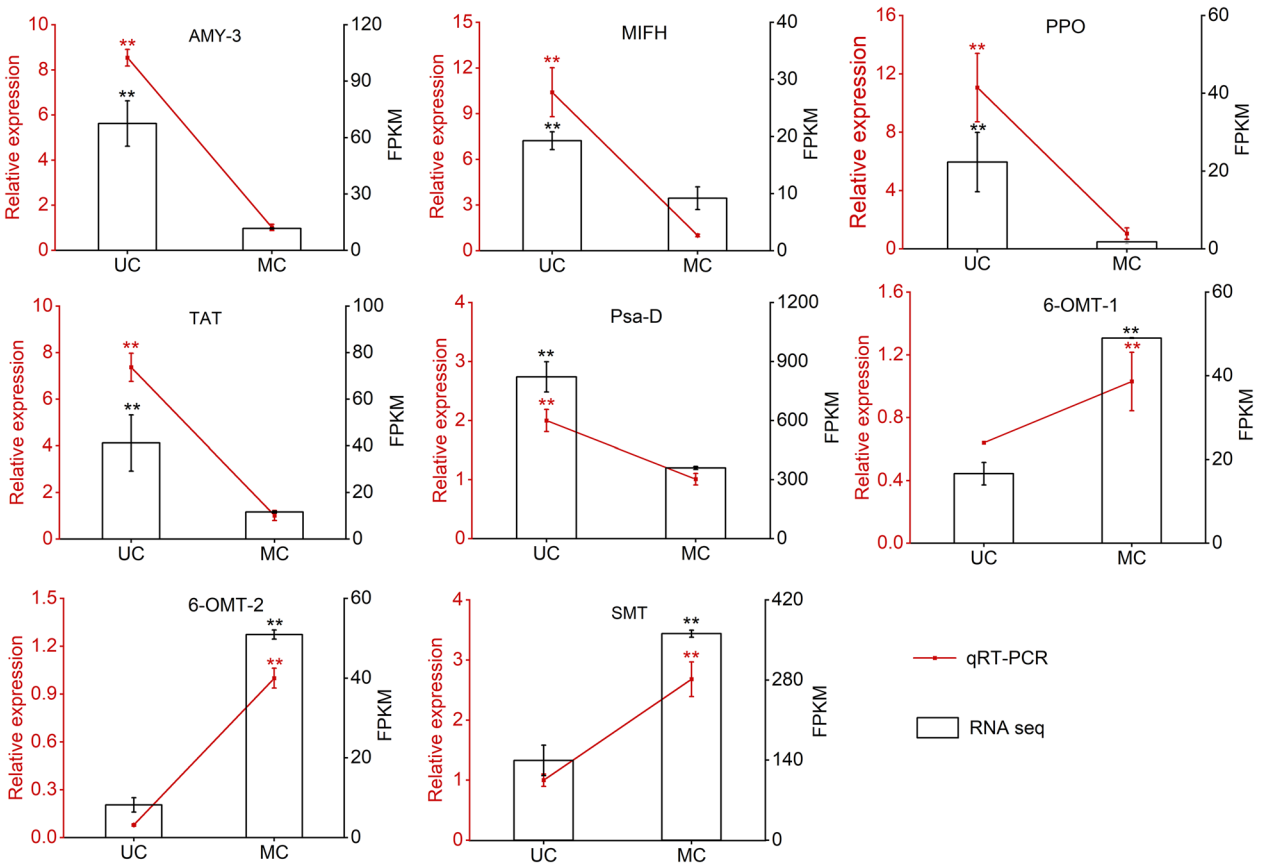

Fig. 10 qRT–PCR validation of eight DEGs involved in the isoquinoline alkaloid biosynthesis and starch and sucrose metabolism pathways. Data in the figure are presented as mean ± SEM. $^{**}p < 0.01$

peroxidation in *C. chinensis* [12, 23]. Under UC, there is a significant increase in SOD enzyme activity, catalyzing the disproportionation of superoxide-free radical to generate more H_2O_2 and O_2 [22]. Subsequently, POD enzyme activity increases to clear excess H_2O_2 [24]. Alterations in antioxidant enzyme activities improved *C. chinensis* viability in response to intercropping. In addition, soluble sugars, soluble proteins, and starch have multiple cellular functions, including stress responses [25, 26]. This study observed a significant increase in soluble sugar, soluble protein, sucrose, and starch contents in the UC system. These findings suggest that these components may play crucial roles in enhancing the viability of *C. chinensis* under understory cultivation system.

Transcriptomic analyses revealed significant enrichment of DEGs in key pathways such as "phenylpropanoid biosynthesis," "zeatin biosynthesis," "photosynthesis," and "starch and sucrose metabolism," indicating their crucial roles in regulating the viability and yield of *C. chinensis*. Phenylpropanoids, specialized secondary metabolites, are known for their critical involvement in biotic and abiotic stress responses [27]. Wu et al. [28] emphasized the significance of phenylpropanoid biosynthesis in tea defense metabolism and its positive impact on enhancing plant viability in understory cultivation systems. Notably, genes participating in phenylpropanoid biosynthesis, including one *4CL*, two *COMT1*, and thirteen *POD* genes, exhibited upregulation in the UC group. The observed increase in POD activity further suggests the crucial involvement of these genes in enhancing the viability of *C. chinensis* [29–31]. Photosynthesis, a fundamental process influencing crop biomass and yield [32], was also impacted in response to understory cultivation. Twenty genes, including *Psb B*, *Psb O*, *Psb R*, *Psb S*, *Psa D*, *Psa E*, *Psa F*, *Psa G*, *Psa H*, *Psa K*, *Psa N*, *Psa O*, *Pet C*, *Pet E*, *Pet F*, *gamma*, *delta*, and *b*, identified in the photosynthesis pathway, exhibited upregulation. These genes may play pivotal roles in the regulation of photosynthesis and yield in *C. chinensis* [31, 32]. Furthermore, sucrose and starch metabolism, crucial for providing nutrients and energy for crop yield and stress responses [33], demonstrated significant alterations in the UC. SS and SPS play crucial roles in the transformation of fructose and glucose into sucrose [34]. SS activity exhibited a substantial increase, and SPS activity showed a slight elevation, indicating their essential roles in regulating sucrose and starch metabolism. The expression of genes associated with sucrose and starch metabolism, including *INV*, *AGL*, *BGL*, *SPS*, *AMY*, and *ISA,* was significantly altered in UC, indicating their potential roles in enhancing yield and viability. Cytokinins, hormones crucial for plant growth and development primarily produced mainly through zeatin biosynthesis [35], also exhibited significant alterations in the UC. In particular, CYP 735A can catalyze trans-zeatin biosynthesis, whereas CKX catalyzes zeatin glycosylation to regulate active cytokinins [36]. Genes such as *CYP 735A*, *CKX5*, *CKX3*, *ZOG*, and *UGT 73C5* significantly differentially expressed, indicating their potential the growth and development of *C. chinensis*. In addition, the DEGs annotated various TFs, including ERF/DREB, WRKY, HD-ZIP, MYB, MIKC C4-GATA-related, GARP_G2-like, SBP, DOF, and AP2, may play pivotal roles in enhancing the viability and yield of the understory cultivation system.

Isoquinoline alkaloids, such as coptisine, epiberberine, palmatine, and berberine, constitute the primary phytochemicals in *C. chinensis* [1]. This study revealed that epiberberine, palmatine, and berberine concentrations notably elevated in the UC compared to the MC, while coptisine exhibited a contrasting trend. The cultivation method positively influenced the levels of epiberberine, palmatine, and berberine, while diminishing coptisine content in *C. chinensis*. In isoquinoline alkaloid biosynthesis, key enzymes such as TAT, TYDC, and PPO play crucial roles. TAT facilitates the conversion of tyrosine to generate 4-hydroxyphenylpyruvate [37], while PPO oxidizes l-tyrosine to generate L-DOPA [38]. TYDC is pivotal in catalyzing the conversion of tyrosine and L-DOPA to form dopamine [1]. This study noted significant upregulation of *TAT*, *TYDC2*, and *PPO* genes in UC, correlating with the increased levels of in epiberberine, palmatine, and berberine. These findings suggest that these genes contribute positively to the accumulation of these phytochemicals. *O*-Methyltransferases (OMTs) have been proposed as essential enzymes in isoquinoline alkaloid biosynthesis [39, 40]. Interestingly, our study noted a significant downregulation of *6-OMT* and *SMT* in UC, consistent with the observed decrease in coptisine. This implies a potential positive regulatory role for these genes in coptisine accumulation. In addition, since isoquinoline alkaloids derive from tyrosine the enrichment of genes related to tyrosine metabolism in our transcriptomic results suggests the involvement of tyrosine metabolism in isoquinoline alkaloid biosynthesis in *C. chinensis*. Notably, the upregulation of *HPPD* and *MIFH* in UC indicates their potential significance in isoquinoline alkaloid biosynthesis under understory cultivation conditions.

Pearson's correlation analyses, a widely employed method for predicting relationships between gene expression and traits [11, 40], have been instrumental in elucidating various biological phenomena. In a study by Wang et al. [40], Pearson's *r* values were calculated between candidate gene expression levels and metabolite intensity, identifying four genes potentially responsible for

raffinose biosynthesis. In our current study, a multitude of genes, including *INV*, *BGL-2*, *BGL-4*, *SPS-2*, *AMY-3*, *Psb B*, *Psb R*, *Psb S*, *Psa D*, *Psa E*, *Psa H*, *Psa O*, *Pet C*, *Pet H*, *deta*, and *b*, exhibited significant positive correlations with plant fresh weight, aboveground fresh weight, and underground fresh weight. This further substantiates the pivotal roles these DEGs may play in yield accumulation. Interestingly, *6-OMT-2* and *COMT1-3* demonstrated significant positive correlations with coptisine content but negative correlations with epiberberine, palmatine, and berberine content. This suggests a potential positive role for these genes in coptisine accumulation but a negative impact on the accumulation of the latter three isoquinoline alkaloids. Similarly, *ZOG-1*, *ZOG-3*, *TAT*, *PPO*, *POD-13*, and *UGT 73C5-1* exhibited significant positive correlations with berberine content, while *MIFH*, *POD-4*, *POD-5*, and *POD-8* showed significant positive correlations with epiberberine, palmatine, and berberine content. Conversely, *POD-5* and *POD-7* displayed significant negative correlations with coptisine content. These intricate relationships highlight the complex roles these DEGs may play in isoquinoline alkaloid accumulation. Notably, SOD activity, POD activity, and MDA content were significantly and positively correlated with epiberberine, palmatine, and berberine content. Likewise, Chl a, Chl b, Chl, Cars, soluble protein, soluble sugar content, starch content, sucrose content, and SS activity exhibited significant positive correlations with individual plant, aboveground, and underground fresh weights. These findings underscore the multifaceted interplay between gene expression levels and physiological properties in the growth and isoquinoline alkaloid accumulation of *C. chinensis*. However, to unravel the intricacies of these relationships, future studies should focus on the functional characterization of these genes through molecular cloning, protein expression, and biochemical assays. Such endeavors will contribute to a deeper understanding of how *C. chinensis* responds to understory cultivations.

Conclusion

This study represents the inaugural exploration into the symbiotic relationship between *C. chinensis* and *C. lanceolata*, revealing a substantial augmentation in the viability, yield, and epiberberine, palmatine, and berberine contents of *C. chinensis*. Intriguingly, coptisine content experienced a notable reduction. The pivotal pathways influencing these outcomes encompass "phenylpropanoid biosynthesis," "zeatin biosynthesis," "photosynthesis," "tyrosine metabolism," "isoquinoline alkaloid biosynthesis" and "starch and sucrose metabolism." Noteworthy contributors to yield accumulation include *INV*, *BGL-2*, *BGL-4*, *SPS-2*, *AMY-3*, *Psb B*, *Psb R*, *Psb S*, *Psa D*, *Psa E*, *Psa H*, *Psa O*, *Pet C*, *Pet H*, *deta*, and *b*. Further nuances emerge as *6-OMT-2* and *COMT1-3* exhibit a positive impact on coptisine content but a negative influence on epiberberine, palmatine, and berberine content. Similarly, *ZOG-1*, *ZOG-3*, *TAT*, *PPO*, *POD-13*, *UGT 73C5-1*, *MIFH*, *POD-4*, *POD-5*, *POD-8*, *POD-5*, and *POD-7* navigate intricate roles in isoquinoline alkaloid accumulation. The dynamic interplay between gene expression and physiological properties emerges as a crucial determinant in the growth and isoquinoline alkaloid accumulation of *C. chinensis* under understory cultivation. These revelations stand as valuable insights for the enhancement of *C. chinensis* yield and quality through strategic understory cultivation practices.

Abbreviations

DEG	Differentially expressed gene
WGCNA	Weighted gene co-expression network analysis
MC	*C. chinensis* monocropping
UC	*C. chinensis*–*C. lanceolata* understory cultivation
Chl a	Chlorophyll a
Chl b	Chlorophyll b
Chl	Chlorophyll a + chlorophyll b
Car	Carotenoid
POD	Peroxidase
SOD	Superoxide dismutase
MDA	Malondialdehyde
SPS	Sucrose phosphate synthase
SS	Sucrose synthase (synthetic direction)
HPLC	High-performance liquid chromatography
KEGG	Kyoto Encyclopedia of Genes and Genomes
TF	Transcription factor gene family
qRT–PCR	Quantitative reverse transcription–polymerase chain reaction
4CL	4-Coumarate-CoA ligase
COMT1	Caffeic acid 3-*O*-methyltransferase
CYP 735A	Cytokinin hydroxylase
CKX5	Cytokinin dehydrogenase 5
ZOG	Zeatin *O*-glucosyltransferase
UGT 73C5	UDP-glycosyltransferase 73C5
Psb B	Photosystem II CP47 reaction center protein
Psb O	Oxygen-evolving enhancer protein 1
Psb R	Photosystem II 10 kDa polypeptide
Psb S	Photosystem II 22 kDa protein
Psa	Photosystem I reaction center subunit
Pet C	Cytochrome b6-f complex iron–sulfur subunit
Pet E	Plastocyanin A
Pet F	Ferredoxin-3
TAT	Tyrosine aminotransferase
TYDC2	Tyrosine/dopa decarboxylase 2
PPO	Polyphenol oxidase
HPPD	4-Hydroxyphenylpyruvate dioxygenase
MIFH	Macrophage migration inhibitory factor homolog
6-OMT	(*S*)-Norcoclaurine 6-*O*-methyltransferase
SMT	(*S*)-Scoulerine 9-*O*-methyltransferase
INV	Beta-fructofuranosidase
AGL	Alpha-glucosidase
BGL	Beta-glucosidase
AMY	Alpha-amylase
ISA	Isoamylase

Supplementary Information

The online version contains supplementary material available at https://doi.org/10.1186/s40538-024-00548-2.

Additional file 1: Figure S1. GO classification histogram. **Figure S2.** Classifications and proportions of TFs. **Figure S3.** Pearson's correlations among physiological properties, yield indicators, and isoquinoline alkaloid contents. A. Pearson's correlations between physiological properties and isoquinoline alkaloid contents. B. Pearson's correlations between physiological properties and yield indicators. Pearson's *r* value was calculated (*, $p < 0.05$; **, $p < 0.01$; ***, $p < 0.001$). Chl a, chlorophyll a; Chl b, chlorophyll b; Chl, chlorophyll a + chlorophyll b; Car, carotenoid; SP, soluble protein content; SS, sugar content. EPI, epiberberine content; COP, coptisine content; PAL, palmatine content; BER, berberine content; PH, plant height; PFW, plant fresh weight; AFW, aboveground fresh weight; UFW, underground fresh weight. **Figure S4.** Linear regression of RNA-Seq and qRT–PCR data that are expressed as a $\log_2$ fold change.

Additional file 2: Table S1. Primer pairs used for qRT–PCR analysis. **Table S2.** Overview of the RNA-Seq data. **Table S3.** DEGs identified in the phenylpropanoid biosynthesis pathway. **Table S4.** DEGs identified in the zeatin biosynthesis pathway. **Table S5.** DEGs identified in the photosynthesis pathway. **Table S6.** DEGs identified in the tyrosine metabolism and isoquinoline alkaloid biosynthesis pathways. **Table S7.** DEGs identified in the starch and sucrose metabolism pathway. **Table S8.** Pearson's correlations between DEGs and yield indicators. **Table S9.** Pearson's correlations between DEGs and isoquinoline alkaloid contents. **Table S10.** Genes selected for qRT–PCR validation. **Table S11.** RNA-Seq and qRT–PCR data used for linear regression.

Acknowledgements
Not applicable.

Author contributions
YD and DY contributed to methodology, formal analysis, and writing—original draft preparation. JW, FW and XG were involved in investigation, validation, and data curation.TT contributed to software utilization, formal analysis, and investigation. XW was involved in software utilization and data curation. SM contributed to investigation and validation. QW and XN were involved in conceptualization and funding acquisition. JG contributed to conceptualization, funding acquisition, supervision, and writing—review and editing.

Funding
This work was funded by the Key Research and Development Plan Project of Hubei (2022BBA153), Hubei Provincial Natural Science Foundation of China (2023 AFB787), the Hubei Technology Innovation Center for Agricultural Sciences—Key Research and Development Project of Science and Technology (2020-620-000-002-04), the Hubei Central Government Guided Local Science and Technology Development Project (2022BGE256), the China Agriculture Research System (CARS-21), the National Key R&D Program of China (2023YFD1600400), Hubei Provincial Seed Industry High Quality Development Special Project (HBZY2023B00506), and the Enshi Prefecture "Disclosure System" Technology Project (D20220093).

Availability of data and materials
The data sets used and/or analyzed during the current study are available from the corresponding author on reasonable request.

Declarations

Competing interests
The authors declare that they have no competing interests.

Author details
[1]Key Laboratory of Biology and Cultivation of Chinese Herbal Medicines, Ministry of Agriculture and Rural Affairs, Institute of Chinese Herbal Medicines, Hubei Academy of Agricultural Sciences, Enshi 445000, China. [2]Hubei Engineering Research Center of Under-Forest Economy, Hubei Academy of Agricultural Sciences, Wuhan 430064, China. [3]Hubei Engineering Research Center of Good Agricultural Practices (GAP) Production for Chinese Herbal Medicines, Institute of Chinese Herbal Medicines, Hubei Academy of Agricultural Sciences, Enshi 445000, China. [4]School of Pharmacy, Xi'an Jiaotong University, Xi'an 710000, China.

Received: 9 December 2023 Accepted: 10 February 2024
Published online: 15 February 2024

References

1. Chen H, Deng C, Nie H, Fan G, He Y. Transcriptome analyses provide insights into the difference of alkaloids biosynthesis in the Chinese goldthread (*Coptis chinensis* Franch.) from different biotopes. PeerJ. 2017;5: e3303. https://doi.org/10.7717/peerj.3303.
2. Liu XM, Tan JP, Cheng SY, Chen ZX, Ye JB, Zheng JR, Xu F, Zhang WW, Liao YL, Yang XY. Comparative transcriptome analysis provides novel insights into the molecular mechanism of berberine biosynthesis in *Coptis chinensis*. Sci Hortic. 2022;291: 110585. https://doi.org/10.1016/j.scienta.2021.110585.
3. Hao Y, Huo J, Wang T, Sun G, Wang W. Chemical profiling of *Coptis* rootlet and screening of its bioactive compounds in inhibiting *Staphylococcus aureus* by UPLC-Q-TOF/MS. J Pharm Biomed. 2020;180: 113089. https://doi.org/10.1016/j.jpba.2019.113089.
4. Tang T, Wang FF, Fang GB, Mao T, Guo J, Kuang H, Sun G, Guo XL, Duan YY, You JM. *Coptischinensis* Franch root rot infection disrupts microecological balance of rhizosphere soil and endophytic microbiomes. Front Microbiol. 2023;14:1180368. https://doi.org/10.3389/fmicb.2023.1180368.
5. Teng H, Choi YH. Optimization of ultrasonic-assisted extraction of bioactive alkaloid compounds from rhizoma coptidis (*Coptis chinensis* Franch.) using response surface methodology. Food Chem. 2014;142:299–305. https://doi.org/10.1016/j.foodchem.2013.06.136.
6. Wang Y, Mo YR, Tan J, Wu LX, Pan Y, Chen XD. Effects of growing *Coptis chinensis* Franch in the natural understory vs under a manmade scaffold on its growth, alkaloid contents, and rhizosphere soil microenvironment. PeerJ. 2022;10: e13676. https://doi.org/10.7717/peerj.13676.
7. Naud J, Olivier A, Bélanger A, Lapointe L. Medicinal understory herbaceous species cultivated under different light and soil conditions in maple forests in southern Québec, Canada. Agroforest Syst. 2010;79:303–26. https://doi.org/10.1007/s10457-009-9262-6.
8. Tong AZ, Liu LJ, Liu W, Qin JM. Comparative analysis of microbial community structure in different times of *Panax ginseng* Rhizosphere microbiome and soil properties under larch forest. BMC Genomic Data. 2023;24:51. https://doi.org/10.1186/s12863-023-01154-1.
9. Kurepin LV, Ivanov AG, Zaman M, Pharis RP, Hurry V, Hüner NP. Interaction of glycine betaine and plant hormones: protection of the photosynthetic apparatus during abiotic stress. In: Photosynthesis: structures, mechanisms, and applications. Cham: Springer; 2017. p. 185–202.
10. Brooker RW, Bennet AE, Cong WF, Daniell TJ, George TS, Hallett PD, Hawes C, Iannetta PP, Jones HG, Karley AJ. Improving intercropping: a synthesis of research in agronomy, plant physiology and ecology. New Phytol. 2015;206(1):107–17. https://doi.org/10.1111/nph.13132.
11. Duan YY, Liu XH, Wu JQ, You JM, Wang FF, Guo X, Tang T, Liao MY, Guo J. Transcriptomic and metabolic analyses reveal the potential mechanism of increasing steroidal alkaloids in *Fritillaria hupehensis* through intercropping with *Magnolia officinalis*. Front Plant Sci. 2022;13: 997868. https://doi.org/10.3389/fpls.2022.997868.
12. Zhou WX, Jiang XG, Tan XH, Li DR, Wang H, You JW, Li XL, Zhang MD. Transcriptome analysis provides novel insights into the soil amendments induced response in continuously cropped *Codonopsis tangshen*. Front Plant Sci. 2022;13: 972804. https://doi.org/10.3389/fpls.2022.972804.
13. Liu YF, Wang B, Shu SH, Li Z, Song C, Liu D, Niu Y, Liu J, Zhang J, Liu H. Analysis of the *Coptis chinensis* genome reveals the diversification of protoberberine-type alkaloids. Nat Commun. 2021;12(1):3276. https://doi.org/10.1038/s41467-021-23611-0.
14. Shi HR, Wang B, Yang PJ, Li YB, Miao F. Differences in sugar accumulation and mobilization between sequential and non-sequential senescence wheat cultivars under natural and drought conditions. PLoS ONE. 2016;11(11): e0166155. https://doi.org/10.1371/journal.pone.0166155.
15. Kim D, Langmead B, Salzberg SL. HISAT: a fast spliced aligner with low memory requirements. Nat Methods. 2015;12(4):357–60. https://doi.org/10.1038/nmeth.3317.
16. Pertea M, Pertea GM, Antonescu CM, Chang TC, Mendell JT, Salzberg SL. StringTie enables improved reconstruction of a transcriptome from

RNA-seq reads. Nat Biotechnol. 2015;33(3):290–5. https://doi.org/10.1038/nbt.3122.
17. Love MI, Huber W, Anders S. Moderated estimation of fold change and dispersion for RNA-seq data with DESeq2. Genome Biol. 2014;15(12):1–21. https://doi.org/10.1186/s13059-014-0550-8.
18. Xie C, Mao XZ, Huang JH, Ding Y, Wu J, Dong S, Kong L, Gao G, Li CY, Wei L. KOBAS 2.0: a web server for annotation and identification of enriched pathways and diseases. Nucleic Acids Res. 2011;39(suppl_2):316–22. https://doi.org/10.1093/nar/gkr483.
19. Duan YY, Wu JQ, Wang FF, Zhang KQ, Guo XL, Tang T, Mu S, You JM, Guo J. Transcriptomic and metabolomic analyses provide new insights into the appropriate harvest period in regenerated bulbs of *Fritillaria hupehensis*. Front Plant Sci. 2023;14:1132936. https://doi.org/10.3389/fpls.2023.1132936.
20. Hasnain M, Chen JW, Ahmed N, Memon S, Wang L, Wang Y, Wang P. The effects of fertilizer type and application time on soil properties, plant traits, yield and quality of tomato. Sustainability. 2020;12(21):9065. https://doi.org/10.3390/su12219065.
21. Liu H, Zhu QD, Pei XX, Xing G, Ou X, Li H. Comparative analysis of the photosynthetic physiology and transcriptome of a high-yielding wheat variety and its parents. Crop J. 2020;8(6):1037–48. https://doi.org/10.1016/j.cj.2020.01.004.
22. Zhou YY, Wang YS, Inyang AI. Ecophysiological differences between five mangrove seedlings under heavy metal stress. Mar Pollut Bull. 2021;172:112900. https://doi.org/10.1016/j.marpolbul.2021.112900.
23. Wang MY, Wu CN, Cheng ZH. Growth and physiological changes in continuously cropped eggplant (*Solanum melongena* L.) upon relay intercropping with garlic (*Allium sativum* L.). Front Plant Sci. 2015;6:262. https://doi.org/10.3389/fpls.2015.00262.
24. Altaf MA, Shahid RS, Ren MX, Naz S, Altaf MM, Khan LU, Tiwari RK, Lal MK, Shahid MA, Kumar R. Melatonin improves drought stress tolerance of tomato by modulating plant growth, root architecture, photosynthesis, and antioxidant defense system. Antioxidants. 2022;11(2):309. https://doi.org/10.3390/antiox11020309.
25. Castro-Cegrí A, Carvajal F, Osorio S, Jamilena M, Garrido D, Palma F. Postharvest abscisic acid treatment modulates the primary metabolism and the biosynthesis of t-zeatin and riboflavin in zucchini fruit exposed to chilling stress. Postharvest Biol Technol. 2023;204: 112457. https://doi.org/10.1016/j.postharvbio.2023.112457.
26. Li CH, Li YH, Chu PY, Zhao HH, Wei ZM, Cheng Y, Liu XX, Zhao FZ, Li YJ, Zhang ZW, Zheng Y, Mu ZS. Effects of salt stress on sucrose metabolism and growth in Chinese rose (*Rosa chinensis*). Biotechnol Biotechnol Equip. 2022;36(1):706–16. https://doi.org/10.1080/13102818.2022.2116356.
27. Vogt T. Phenylpropanoid biosynthesis. Mol Plant. 2010;3(1):2–20. https://doi.org/10.1093/mp/ssp106.
28. Wu T, Jiang Y, Li M, Pu D, Shi M, Lan ZQ. RNA-seq analysis reveals the potential mechanism of improved viability and product quality of tea plants through intercropping with Chinese chestnut. Plant Growth Regul. 2022;96:177–93. https://doi.org/10.1007/s10725-021-00768-8.
29. Chen XH, Wang HT, Li XY, Ma K, Zhan Y, Zeng F. Molecular cloning and functional analysis of 4-Coumarate: CoA ligase 4 (4CL-like 1) from *Fraxinus mandshurica* and its role in abiotic stress tolerance and cell wall synthesis. BMC Plant Biol. 2019;19:1–16. https://doi.org/10.1186/s12870-019-1812-0.
30. Liang SM, Xu SB, Qu D, Yang L, Wang J, Liu H, Xin W, Zou D, Zheng H. Identification and functional analysis of the caffeic acid *O*-methyltransferase (COMT) gene family in rice (*Oryza sativa* L.). Int J Mol Sci. 2022;23(15):8491. https://doi.org/10.3390/ijms23158491.
31. Zhou WX, Duan YY, Jiang XG, Tan XH, Li Q, Wang H, Zhang YJ, Zhang MD. Transcriptome and metabolome analyses reveal novel insights into the seed germination of *Michelia chapensis*, an endangered species in China. Plant Sci. 2023;328: 111568. https://doi.org/10.1016/j.plantsci.2022.111568.
32. Simkin AJ, Faralli M, Ramamoorthy S, Lawson T. Photosynthesis in non-foliar tissues: implications for yield. Plant J. 2020;101(4):1001–15. https://doi.org/10.1111/tpj.14633.
33. Zeng RE, Chen TT, Wang XY, Cao J, Li X, Xu X, Chen L, Xia Q, Dong Y, Huang L. Physiological and expressional regulation on photosynthesis, starch and sucrose metabolism response to waterlogging stress in peanut. Front Plant Sci. 2021;12: 601771. https://doi.org/10.3389/fpls.2021.601771.
34. Zhang Q, Tang FX, Cai WC, Peng B, Ning M, Shan CH, Yang XQ. Chitosan treatment reduces softening and chilling injury in cold-stored Hami melon by regulating starch and sucrose metabolism. Front Plant Sci. 2022;13:1096017. https://doi.org/10.3389/fpls.2022.1096017.
35. Sasaki E, Ogura T, Takei K, Kojima M, Kitahata N, Sakakibara H, Asami T, Shimada Y. Uniconazole, a cytochrome P450 inhibitor, inhibits trans-zeatin biosynthesis in *Arabidopsis*. Phytochemistry. 2013;87:30–8. https://doi.org/10.1016/j.phytochem.2012.11.023.
36. Guo SH, Chen YC, Zhu YX, Tian M. Transcriptome analysis reveals differentially expressed genes involved in somatic embryogenesis and podophyllotoxin biosynthesis of *Sinopodophyllum hexandrum* (Royle) T.S. Ying. Protoplasma. 2023;260:1221–32. https://doi.org/10.1007/s00709-023-01843-9.
37. Liu XC, Tang YL, Zeng JL, Qin J, Lin M, Chen M, Liao Z, Lan X. Biochemical characterization of tyrosine aminotransferase and enhancement of salidroside production by suppressing tyrosine aminotransferase in *Rhodiola crenulata*. Ind Crop Prod. 2021;173: 114075. https://doi.org/10.1016/j.indcrop.2021.114075.
38. Noori R, Perwez M, Mazumder JA, Ali J, Sardar M. Bio-imprinted magnetic cross-linked polyphenol oxidase aggregates for enhanced synthesis of L-dopa, a neurodegenerative therapeutic drug. Int J Biol Macromol. 2023;227:974–85. https://doi.org/10.1016/j.ijbiomac.2022.11.274.
39. Inui T, Tamura KI, Fujii N, Morishige T, Sato F. Overexpression of *Coptis japonica* norcoclaurine 6-*O*-methyltransferase overcomes the rate-limiting step in benzylisoquinoline alkaloid biosynthesis in cultured *Eschscholzia californica*. Plant Cell Physiol. 2007;48(2):252–62. https://doi.org/10.1093/pcp/pcl062.
40. Wang H, Asker K, Zhan C, Wang N. Transcriptomic and metabolic analysis of fruit development and identification of genes involved in raffinose and hydrolysable tannin biosynthesis in walnuts. J Agric Food Chem. 2021;69(28):8050–62. https://doi.org/10.1021/acs.jafc.1c02434.

Publisher's Note